Supporting Information

Carbon Fabric Supported 3D Cobalt Oxides/Hydroxide Nanosheet Network as Cathode for Flexible All-Solid-State Asymmetric Supercapacitor

Tianfeng Qin,[a] Shan Dang,[a] Jiaxin Hao,[a] Zilei Wang,[a] Haoqian Li,[a] Yuxiang Wen,[a] Shuqi Lu,[a] Deyan He, [a] Guozhong Cao,*[b] Shanglong Peng*[a]

[a] School of Physical Science and Technology and Key Laboratory for Magnetism and Magnetic Materials of the Ministry of Education, Lanzhou University, Lanzhou 730000, P.R. China. E-mail: pengshl@lzu.edu.cn;

[b] Department of Materials Science and Engineering, University of Washington, Seattle, Washington 98195-2120, United States. E-mail: gzcao@u.washington.edu.

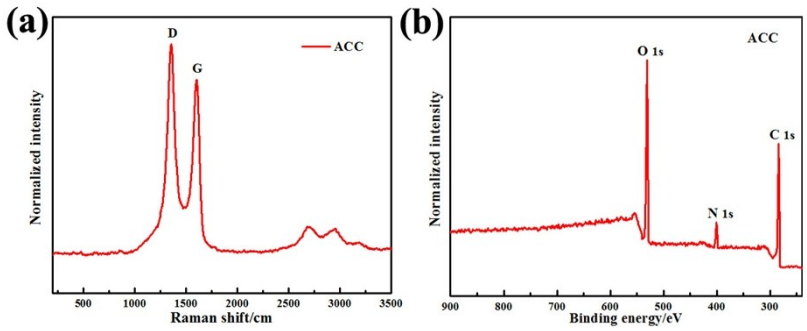

Fig. S1. (a) Raman and (b) XPS spectra of ACC substrate.

Table S1 Capacitance comparison of this work with previously reported literatures

Electrode	Highest capacitance/(F g^{-1})	Reference
Ni-Co-precursor	400 at 1 A g^{-1}	1
Hollow Co_3O_4 nanowire arrays	599 at 2 A g^{-1}	2
Co_3O_4 nanosheets	500 at 1.25 A g^{-1}	3
Needle-like Co_3O_4/graphene	158 at 0.1 A g^{-1}	4
Co_3O_4@ MnO_2	530 at 0.5 A g^{-1}	5

Nano-Co_3O_4@Au nanoparticles	681 at 0.5 A g^{-1}	6
3 D-network Co oxides/hydroxide	711 at 1 A g^{-1}	This work

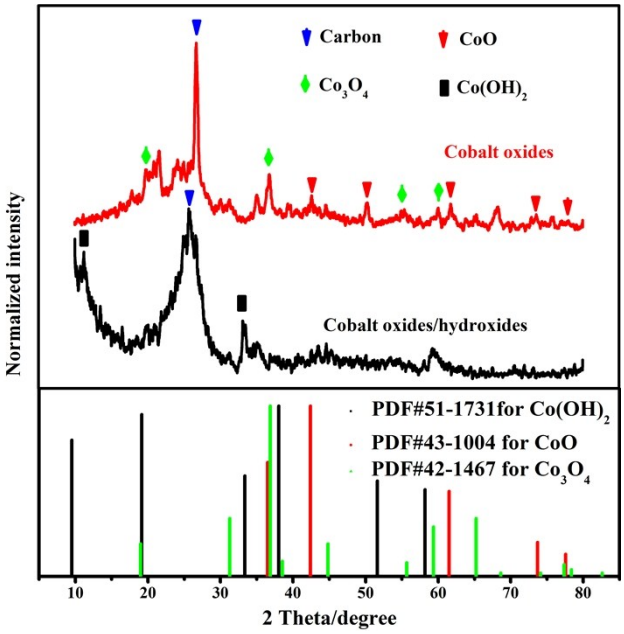

Fig. S2. XRD patterns of the cobalt oxides/hydroxide and the cobalt oxides control samples.

Fig. S2 displays XRD patterns with the wide range from 10° to 80° for cobalt oxides/hydroxide and cobalt oxides samples. The strongest peak centered at ~ 26° derives from the active carbon cloth (ACC) confirmed. Peaks in the XRD curve of the cobalt oxides/hydroxide are well indexed to hexagonal phase $Co(OH)_2$ (PDF#51-1731), cubic phase single crystal Co_3O_4 (PDF#42-1467) and cubic phase CoO (PDF#43-1004). After annealing in Ar at 430 °C for 3 hours (denoted as cobalt oxides sample), the characteristic peaks of hexagonal phase $Co(OH)_2$ located at 11.25° and 33.34° disappears due to the irreversible transformation of $Co(OH)_2$ to Co oxide. Moreover, the intensity of other cobalt oxides (CoO and Co_3O_4) peaks becomes more sharp, indicative of a higher crystalline for the annealed sample.

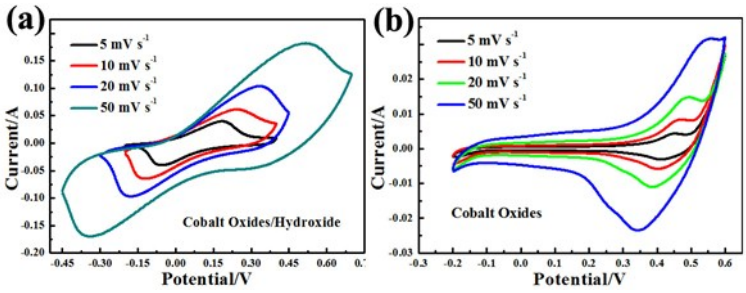

Fig. S3. CV curves of (a) the Co oxides/hydroxide and (b) the Co oxides with the scan rates from 5 mV s^{-1} to 50 mV s^{-1}.

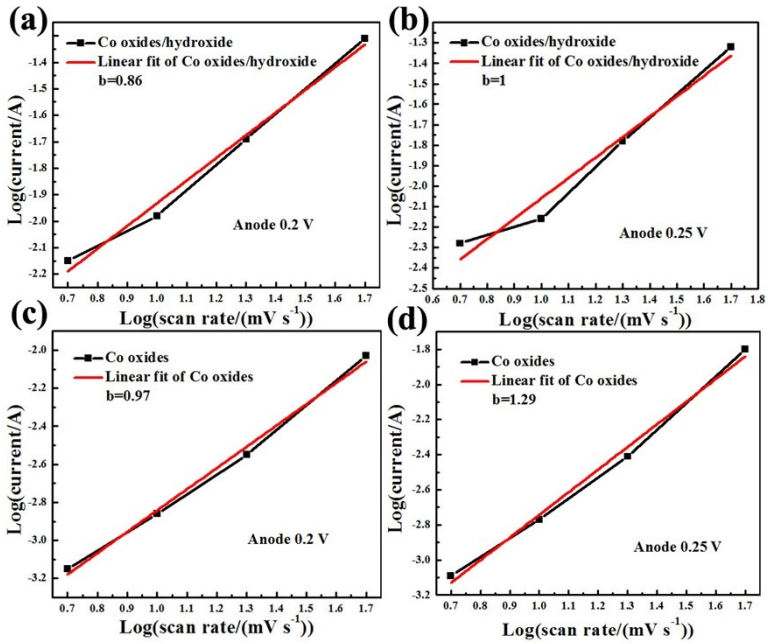

Fig. S4. The linear dependence of log current on log sweep rate (based on Equation (2)) for (a,b) Co oxides/hydroxide at 0.2 V and 0.25 V and (c,d) Co oxides at 0.2 V and 0.25 V during the correspondingly anodic CV processes.

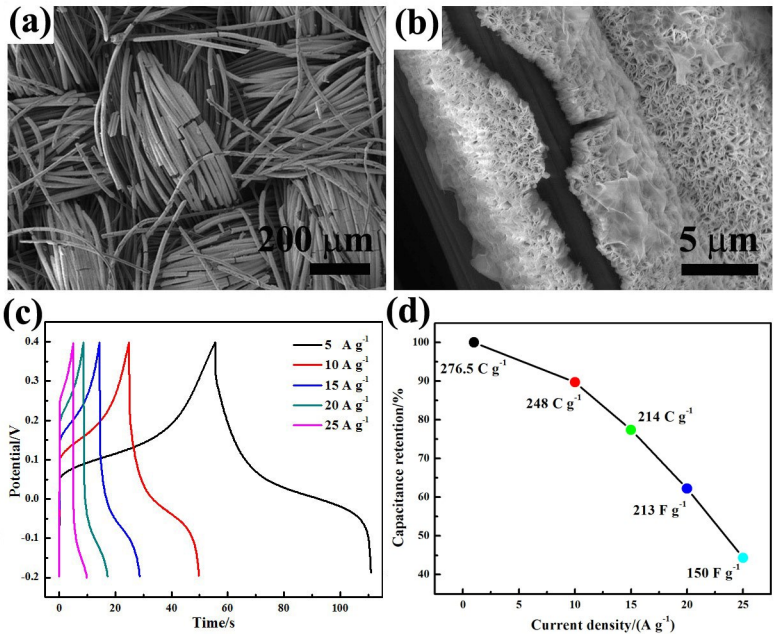

Fig. S5. Characterizations of the prepared sample using hydrophobic carbon cloth (CC) as substrate. (a) Low and (b) high-magnification SEM images. (c) GCD curves with the current densities from 5 to 25 A g^{-1} and (d) capacity as a function of current density.

In our experiment, a simple electrochemical oxidation method was employed to make hydrophobic carbon cloth hydrophilic to enhance the electrochemical performance. Low-magnification SEM image in Fig. S3(a) shows that the surface of hydrophobic carbon fiber just is partially coated by ruptured active materials (Co oxides/hydroxides). Compared to SEM image of sample with ACC substrate (treated CC using concerned H_2SO_4) in Fig. 1(b), the crevice with the size of ~1 um is observed as shown in Fig. S3(b), indicating worse contact between hydrophobic carbon fiber and active materials. GCD test electrode was carried out at different current densities in Fig. S3(c). Shorter voltage platforms and charge/discharge time with increased current density are obtained compared to that of 50^{o}C/10C/ACC electrode using hydrophilic carbon cloth obtained by electrochemical oxidation as substrate in Fig. 3(a). Correspondingly, as shown in Fig. S3(d), the electrode with untreated CC substrate shows lower mass capacities and poor rate ability compared to electrode with ACC substrate (treated CC using concerned H_2SO_4) in Fig. 3(b). Thus, a conclusion here that we obtain is that electrochemical oxidation using concentrated sulfuric acid to hydrophobic carbon cloth remarkably enhances the capacitances and rate ability due to the tighter contact between hydrophilic carbon cloth and active materials.

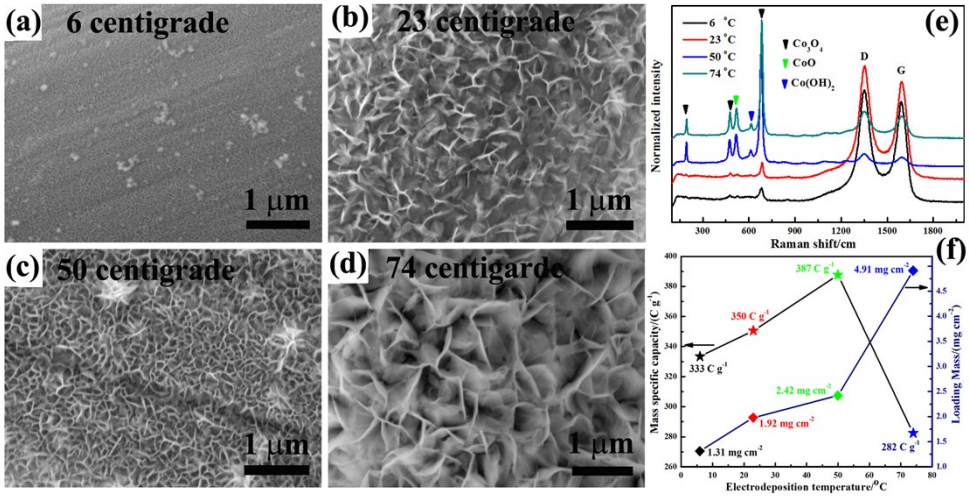

Fig. S6. Effect of electrodeposition temperature on the morphology and electrochemical properties of prepared samples. SEM images of samples prepared at (a) 6°C, (b) 23°C, (c) 50°C and (d) 74°C. (e) Raman spectra of samples prepared at different electrodeposition temperatures. (f) Mass specific capacity and mass loading as a function of electrodeposition temperatures.

The effect of electrodeposition temperature on samples' performance was investigated as shown in Fig. S4 with keeping other parameters unchanged. Fig. S4(a-d) show SEM images of samples prepared at different temperatures (6°C, 23°C, 50°C and 74°C). The nanosheets' size of active materials coated on the surface of carbon fiber gradually become larger and larger with the increasing electrodeposition temperatures from 6 to 74°C. Also, as shown in Fig. S4(c), sample prepared at 50°C indicates the highest cross-linked degree than that of others in Fig. S4(a, b and d). Raman test in Fig. S4(e) was also employed to study the component variation of samples prepared at different electrodeposition temperatures. First, at high wavenumber region, the relative intensity of both D and G bands becomes lower and lower with the increased electrodeposition due to the denser shell of active materials coated on the surface of carbon fiber. On the contrary, at low wavenumber region, the relative intensity of characteristic peaks derived from active materials shows an incremental trend with the increasingly elevated electrodeposition temperatures, also

indicative of denser active materials' formation. The variation of characteristic peaks is observed as shown in Fig. S4(e): for samples prepared at 6 and 23°C, signal peaks of active materials at 480, 526 and 686 cm^{-1} appear in their spectra, corresponding to Co_3O_4 and CoO, respectively (denoted as Fig. S4(e)); new peaks located at 195 and 611 cm^{-1} appear in their spectra, corresponding to Co_3O_4 and $Co(OH)_2$, respectively, while the electrodeposition temperature increases to 50 and 74°C. Finally, GCD test at a current density of 1 A g^{-1} was carried out as shown in Fig. S4(f). With the increasingly elevated temperature (6 °C to 74 °C), the mass loading per unit area also shows the same trend from 1.31 to 4.91 mg cm^{-2}. On the contrary, the mass specific capacity gradually increases to the highest value of 387 C g^{-1} (50 °C) from 333 C g^{-1} (6 °C) but sharply decreases to 282 C g^{-1} while the temperature continuously increases to 74°C, indicating sample prepared at 50 °C has the optimal electrochemical property. Thus, electrodeposition temperature of 50 °C is selected as the optimal temperature.

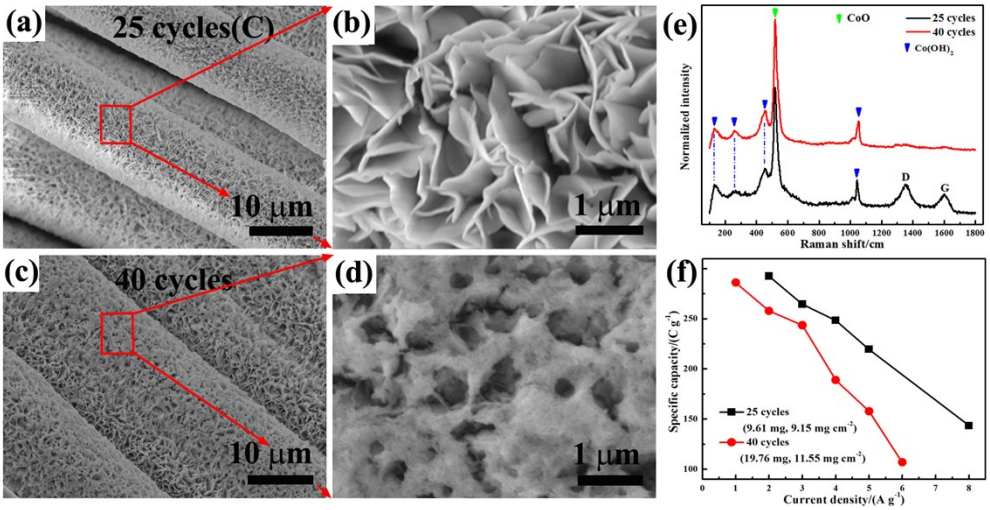

Fig. S7. Effect of electrodeposition cycle number on the morphology and property of samples at 25 and 40 cycles without changing other parameters. (a) Low and (b) high-magnification SEM images of sample. (c) Low and (d) High-magnification SEM images of samples prepared using 40 cycles. (e) Raman spectra of samples prepared using 25 and 40 cycles. (f) Specific capacity as a function of current density.

Also, experiments using different electrodeposition cycle were conducted to obtain the optimal parameter. Fig. S5(a-d) are SEM images of samples prepared by prolonging the cycle number to 25 and 40 cycles. Active materials shell also is coated on the surface of carbon fiber, just indicating a difference in diameter of carbon fiber due to the thicker shell of active materials in Fig. 1(b) of 10 cycles, Fig. S5(a) of 25 cycles and Fig. S5(c) of 40 cycles. Besides, the cross-linked degree and the thickness of nanosheets become lower and thicker, respectively, than that of 10 cycles' sample in Fig. 1(c). High-magnification SEM image of 40 cycles' sample in Fig. S5(d) shows the surface of carbon fiber is coated by dense bulk of active materials with irregular pores, indicating entirely different morphology. Raman spectra in Fig. S5(e) was employed to confirm the component variation of samples. Compared to 10 cycles' sample in Fig. 2(a), the peak signals of Co_3O_4 disappear but remain characteristic peaks of CoO and $Co(OH)_2$ as shown in Fig. S5(e). Also, the capacitance at different current density for different samples is shown in Fig. S5(f). Compared to higher capacity of 427 C g^{-1} (1A g^{-1}) and rate ability of 80% (10 A g^{-1}) for 10 cycles' sample in Fig. 3(b), 25 cycles' and 40 cycles' samples show lower capacitance and worse rate ability such as 280 C g^{-1}(2 A g^{-1}) and 48 % of rate ability (8 A g^{-1}) for 25 cycles' sample, 285 C g^{-1} (1 A g^{-1}) and 37 % of rate ability (6 A g^{-1}) for 40 cycles' sample due to higher mass loading of 25 and 40 cycles' sample (9.15 and 11.55 mg cm^{-2}, respectively) and worse morphology unbeneficial to the transfer of electrolyte ions. Therefore, electrodeposition cycle number of 10 is selected as the optimal parameter.

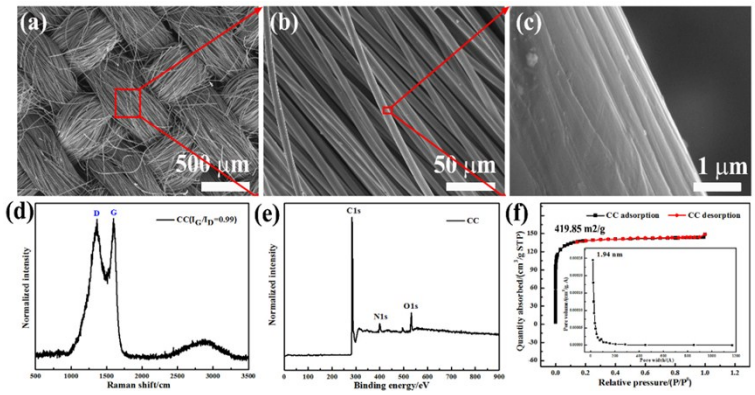

Fig. S8. (a-c) SEM images of carbon cloth with large surface area(CC). The corresponding (d) Raman spectrum, (e) XPS full pattern and (f) Nitrogen adsorption/desorption isotherm curve, inset: pore size distribution spectrum.

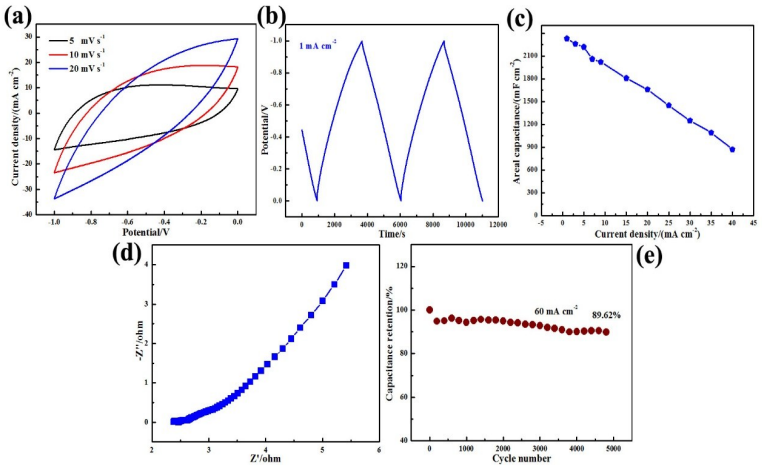

Fig. S9. The electrochemical performances of CC anode in 1 M KOH aqueous solution.

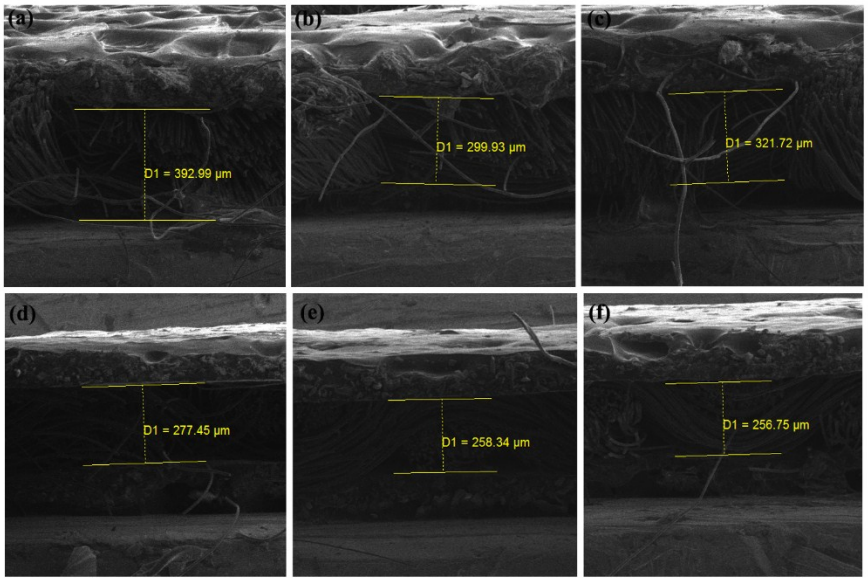

Fig. S10. Thickness of (a-c) cathode and (d-f) anode, in which the average thicknesses of cathode and anode are ~338 um and ~266 um, respectively.

Table S2 Comparison of volume energy density of supercapacitor with previously reported literatures (reference number is indexed from manuscript).

Supercapacitor	Maximum volume energy density/(mWh cm^{-3})	Reference number
Ni/MnO_2-filter paper(FP)//Ni/AC-FP	0.78	46
carbonnanotubes //Fe_3O_4-C	1.56	48
Co_3O_4@C@Ni_3S_2//AC	1.52	49
H-TiO_2@MnO_2//H-TiO_2 @C	0.3	44
Co oxides/Hydroxide//carbon cloth	2.78	This work

References

[1] W. He, C. Wang, H. Li, X. Deng, X. Xu and T. Zhai, *Advanced Energy Materials*, 2017, DOI: 10.1002/aenm.201700983, 1700983.

[2] X.-h. Xia, J.-p. Tu, Y.-j. Mai, X.-l. Wang, C.-d. Gu and X.-b. Zhao, *Journal of Materials Chemistry*, 2011, **21**, 9319.

[3] K. Ding, P. Yang, P. Hou, X. Song, T. Wei, Y. Cao and X. Cheng, *Advanced Materials Interfaces*, 2017, **4**, 1600884.

[4] Q. Guan, J. Cheng, B. Wang, W. Ni, G. Gu, X. Li, L. Huang, G. Yang and F. Nie, *ACS applied materials & interfaces*, 2014, **6**, 7626-7632.

[5] M. Feng, G. Zhang, Q. Du, L. Su, Z. Ma, X. Qin and G. Shao, *Ionics*, 2017, **23**, 1637-1643.

[6] Y. Tan, Y. Liu, L. Kong, L. Kang and F. Ran, *Journal of Power Sources*, 2017, **363**, 1-8.